RSC Advances

PAPER

View Article Online
View Journal | View Issue

Cite this: *RSC Adv.*, 2021, **11**, 37851

Carbon nanotubes/Al_2O_3 composite derived from catalytic reforming of the pyrolysis volatiles of the mixture of polyethylene and lignin for highly-efficient removal of Pb(II)†

Zhanghong Wang,*[ab] Kun Qin,[a] Zhikang Wang,*[a] Dekui Shen*[b] and Chunfei Wu*[c]

In the present study, the coked catalysts derived from catalytic reforming of the pyrolysis volatiles of polyethylene (PE), lignin (LG) and their mixture were developed as low-cost and environmentally-friendly carbon materials-containing composites to remove heavy metal ions from aqueous solution. The composites were thoroughly characterized by SEM, TEM, XRD, TGA and FT-IR and then their adsorption capability towards Pb(II) was investigated. It is found that curved cone-shape carbon nanotubes (CNTs) with abundant structural defects and O-containing surface functional groups, such as C–O, C=O and –OH, can be obtained from the catalytic reforming of the mixture of PE and LG. The CNT-containing catalyst composite presents a superior adsorption capability towards Pb(II) when it is employed in Pb(II) removal. Adsorption isotherm and adsorption kinetics studies show that the adsorption process can be well simulated by the Langmuir isotherm and pseudo-second-order model, demonstrating that the adsorption is subjected to a homogeneous and chemical process. The calculated maximum adsorption capacity is as high as 146.08 mg g^{-1}, which is much higher than most of the adsorbents reported. Moreover, thermodynamic analysis reveals that the adsorption is spontaneous and endothermic. Accordingly, the used catalyst from the catalytic reforming can be developed as a low-cost and highly-efficient adsorbent.

Received 8th September 2021
Accepted 13th November 2021

DOI: 10.1039/d1ra06762a

rsc.li/rsc-advances

1 Introduction

Heavy metal-related contaminants mainly originate from anthropogenic activities such as industrial manufacture, energy production and transportation and are widely pervasive in our surroundings in the forms of dust, precipitation and ions in the air and drinking water.[1,2] It is confirmed that the prolonged exposure to and excessive uptake of heavy metals would cause severe damage to body organs (kidneys, liver and brain), bone, blood and nervous systems due to their acute toxicity, and non-biodegradable and bioaccumulative nature.[3] Accordingly, contamination and corresponding risks arising from heavy metals have attracted a large number of concerns. In the past few decades, strict standards about the limitations of individually toxic heavy metals have successively been set in most countries and important health institutions.[4] For example, the maximum contaminant level for lead (Pb), chromium, cadmium, arsenic, mercury, copper, zinc and nickel in drinking water, several of the most representatives of heavy metals, is 0.01, 0.05, 0.003, 0.01, 0.06, 2, 3 and 0.07 mg g^{-1}, respectively, according to the World Health Organization provisional guidelines.[5] In order to achieve the goals, several methods involving ion exchange, chemical precipitation, reverse osmosis, membrane and ultrafiltration have been successfully developed to address heavy metals-related contaminations. However, most of these techniques show disadvantages such as low efficiency and extra energy or chemical requirements, which greatly limit their flexibility and applicability. By contrast, adsorption has generally been accepted as one of the most promising methods because of its high efficiency, cost-effectiveness, sludge-free and simplicity.[6] Up to now, a large amount of adsorbents has been applied in adsorption techniques, such as virgin biomass, biomass-based carbon materials, clay minerals, ceramics and oxides.[2,7–10]

Carbon nanomaterials, such as CNTs and graphene, possessing high specific surface area and abundant adsorption sites, have been considered as a class of newly emerging and highly efficient adsorbents.[11] However, low dispersity and

[a]*College of Eco-Environmental Engineering, Guizhou Minzu University, Guiyang 550025, PR China. E-mail: z.wang@gzmu.edu.cn; wzk8726@sina.com*

[b]*Key Laboratory of Energy Thermal Conversion and Control of Ministry of Education, Southeast University, Nanjing 210096, PR China. E-mail: 101011398@seu.edu.cn*

[c]*School of Chemistry and Chemical Engineering, Queen's University Belfast, Belfast BT7 1NN, UK. E-mail: c.wu@qub.ac.uk*

† Electronic supplementary information (ESI) available. See DOI: 10.1039/d1ra06762a

strong hydrophobicity arising from their strong Van de Waals force and unique molecular structure have become crucial to restrict the practical applications of carbon nanomaterials to a certain degree. An alternative method to improve the dispersity and hydrophilicity of carbon nanomaterials is to combine with other materials to achieve carbon nanomaterial-contained composites.[12] As a result, the removal efficiency of the carbon nanomaterials serving as adsorbents was found to be greatly improved.[13,14] For example, Ca/Al layered double hydroxide decorated CNTs composites fabricated from CNTs and Ca/Al-containing precursor solution *via* co-precipitation and hydrothermal aged treatment possessed a favorable adsorption capability towards U(VI), which was 4-fold that of pristine CNTs.[15] Similarly, the adsorption ability of graphene oxide towards Cd(II) and Ni(II) was found to be greatly improved as it was incorporated with almond shell (graphene oxide/almond shell composite) by a freeze-drying method.[16]

However, it is worth noting that a complex assembly or synthesis process is generally needed for the preparation of desirable carbon nanomaterials-contained composites, which hence brought a large amount of wastage and cost as well as extra wastes. Interestingly, various carbon nanomaterials-contained composites being considered as by-products or industrial wastes are inevitably and largely being produced in daily industrial production, such as catalytic pyrolysis or reforming-involved industries.[17,18] The used catalysts in these industries are generally deactivated and poisoned by the damage of structure or the production of coke, which are difficult to recover and conduct to further reuse. Further analysis revealed that the coke that existed on the used catalysts is mainly composed of amorphous carbons and ordered structure carbons (carbon nanomaterials).[19] The carbons are uniformly covered or nested on the catalyst surface or its inner pore structure. Also, abundant oxygen-containing functional groups can be found in the carbons in the catalytic conversion of oxygen-contained feedstock, which endowed their favorable hydrophilicity and excellent adsorption sites.[13,20] Therefore, the used catalysts can be sustainably disposed of as a low cost source of carbon nanomaterials-contained composites, employing as an efficient adsorbent for the removal of pollutants from environment.

Herein, the purpose of the present work is to investigate the feasibility and performance for the employment of the carbon nanomaterials-contained composites originated from used catalysts as adsorbents on pollutants removal. Three types of used catalysts derived from catalytic reforming of the vapor of LG, PE and their mixture were comparably investigated to determine the influence of the type of carbon nanomaterials and corresponding surface chemistry, which were characterized by SEM, XRD, TEM, TG and FTIR. The adsorption capability of these three types of used catalysts towards Pb(II) from aqueous solution varied from adsorption conditions, such as initial Pb(II) concentration, contact time, solution pH and ambient temperature were further investigated. Adsorption isotherm, kinetic, thermodynamics and potential adsorption mechanism were analyzed and discussed as well.

2 Materials and methods

2.1 Raw materials and chemicals

LG was extracted from a black liquor collected from an alkali pulping mill in Hunan Province, China, according to an acid precipitate method which has been exhaustively described in our previous study.[21] Commercially available PE powder with an average M_w of ~4000 and M_n of ~1700 GPC was provided by Sigma–Aldrich Corporation (St. Louis, MO, USA). Chemicals including nickel nitrate hexahydrate, aluminium oxide (Al_2O_3), nitric acid, sodium hydroxide, lead nitrate and EDTA in analytical reagent grade were obtained from Sigma-Aldrich Corporation (St. Louis, MO, USA). Deionized water with a resistivity of 18.2 MΩ cm^{-1} was employed as a solvent to prepare the desired solution.

2.2 Preparation of carbon materials/Al_2O_3 composites

2.2.1 Preparation of Al_2O_3 catalyst. Al_2O_3 with 10% Ni content (NiO/Al_2O_3) was employed as the catalytic reforming catalyst. In brief, 4.95 g of nitrate hexahydrate was dissolved into 40 mL ethanol to obtain a Ni-containing solution. Then Al_2O_3 in a mass of 10 g was added and kept stirring for 4 h. After that, the suspension was carried out evaporating under 80 °C. The as-obtained solid was then dried under oven at 105 °C, followed by calcination at 500 °C with a heating rate of 2 °C min^{-1} at air atmosphere. At last, the solid residue was collected and ground to powder, which is right the desired catalyst (NiO/Al_2O_3).

2.2.2 Catalytic reforming the pyrolysis volatiles of LG, PE and their mixture. Catalytic reforming PE, lignin and their mixture (in a mass ratio of 1 : 1) was carried out at a vertical two-stage fixed bed where nitrogen was introduced to maintain an inert atmosphere (Fig. S1†). The feedstock was pyrolyzed at the first stage with a heating rate of 10 °C min^{-1} at 800 °C for 2 h. The produced vapour was passed through the catalyst bed placed in the second stage where the temperature was controlled as 600 °C. Particularly, the first stage was commenced to heat after the catalyst bed reached the set temperature. Once the pyrolysis at the first stage finished, the two stages were simultaneously ceased. Then the instrument was allowed to cool down naturally to room temperature. The reacted catalyst carpeting with carbon materials (carbon materials Ni/Al_2O_3) was collected. Particularly, the carbon materials Ni/Al_2O_3 composites originated from PE, LG and their mixture were labelled as PE-CNTs-Ni/Al_2O_3, LG-Chars-Ni/Al_2O_3 and PE/LG-CNTs-Ni/Al_2O_3, respectively.

2.3 Characterization of as-synthesized carbon materials/Al_2O_3 composites

The crystalline information of carbon products and corresponding catalyst components in samples (the as-synthesized fresh Ni/Al_2O_3 catalysts with different Ni content and carbon materials-Ni/Al_2O_3 composites) was determined by a powder X-ray diffractometer with Cu Kα radiation in the 2θ range 5–80° (Empyrean series 2, PANalytical, Netherlands). The reduction behaviors of the fresh catalysts were detected by a Temperature

Programmed Reduction instrument (TPR) (FineSorb3010, FINETEC instrument, China). Morphologic features of the samples were characterized using scanning electron microscopy (SU1510, Hitachi, Japan). Transmission electron microscope (JEM-2010F, JOEL, Janpan) equipped with a high-resolution transmission electron microscopy (talos F200, FEI, USA) was employed to investigate the detailed morphology of the samples. Thermogravimetric analysis was conducted to determine the thermal stability of samples in the air using a thermo-gravimetric analyzer (SDT Q600, TA instrument, USA) in the temperature range of 30–850 °C with a heating rate of 10 °C min^{-1}. Surface functional groups of the samples were analyzed by a Fourier Transform Infrared Spectrometer (Nicolet iS5, Thermo Fisher Scientific, USA). The vibration of the transmissions and corresponding wavenumbers ranging from 600 to 4000 cm^{-1} were collected with a resolution of 4 cm^{-1}. Ash, volatile matter and fixed carbon of the samples were measured according to the standard method (ASTM D 1762-84). The analysis on the composition of carbon (C), hydrogen (H) and sulphur (S) in samples was carried out on an Elemental Analyzer (EA112, Thermo Finnigan, USA). While the oxygen content (O) was calculated by difference. The specific surface area of samples was determined by N_2 adsorption/desorption at 77 K on a surface area analyzer (NOVA-2000E, Quantachrome Instruments, USA) according to the Brunauer–Emmett–Teller (BET) method. The point of zero charge (pHpzc) of samples was measured based on the method in our previous study.[7]

2.4 Adsorption of Pb(II) onto carbon materials/Al_2O_3 composites

Stock solution of Pb(II) in a concentration of 1000 mg L^{-1} was prepared by dissolving lead nitrate in deionized water. Pb(II)-containing solutions in required initial concentrations were subsequently prepared by diluting the calculated amount of the stock solution to 50 mL using deionized water in 100 mL conical flasks. About 0.05 mg sample (PE-CNTs-Ni/Al_2O_3, LG-Chars-Ni/Al_2O_3 or PE/LG-CNTs-Ni/Al_2O_3) was added to the flasks and shook at a horizontal air bath shaker under 25 °C for 8 h with a constant rate of 120 r/min. Afterwards, the suspensions were filtered with 0.22 μm filters and the separated filtrates were analysed by an atomic adsorption spectrometer (AAS) (FAAS-M6, Thermo, USA) to determine the remnant Pb(II) concentration. The effect of initial concentrations (ranging from 20 to 400 mg L^{-1}), contact time (ranging from 0–8 h), ambient temperature (ranging from 15–45 °C) and solution pH (ranging from 2 to 6) on the adsorption of Pb(II) on samples were extensively investigated. Particularly, the pH of Pb(II) solution was accurately controlled with diluted HNO_3 or NaOH.

For the investigation of reusability, 0.05 g of Pb(II)-loaded PE/LG-CNTs-Ni/Al_2O_3 composites were mixed with 10 mL of 0.1 mol L^{-1} EDTA solution and then ultrasonicated at 25 °C for 10 min to desorb. The suspension was filtered. The Pb(II) concentration in filtrate was determined and the filter residue was dried and employed for the renewed adsorption. Five repeated adsorption–regeneration cycles were performed.

3 Results and discussion

3.1 Characteristics of carbon materials-Ni/Al_2O_3 composites

The SEM images of carbon materials-Ni/Al_2O_3 composites are shown in Fig. 1. Preliminary observations under low magnification reveal that Ni/Al_2O_3 derived from catalytic reforming PE and LG/PE mixture is covered with dense carbon materials (Fig. 1a and c). Further study demonstrates that PE-derived carbon materials show long and entangled fibre-like structures (15–30 μm in length and 5–50 nm in diameter) while stubby and interconnected ones can be found from PE/LG mixture-derived carbon materials (0.1–1 μm in length and 10–100 nm in diameter) in term the result of Fig. 1b and d. It is reported that filamentous carbon materials were found to be the most important and ubiquitous carbon materials during catalytic reforming plastics and their mixture together with biomass.[22,23] For catalytic reforming LG, bulk spine-like structured carbon is obtained, which is evidently different from those from PE and LG/PE mixture. This result is also different from that of Wu, *et al.*, where pyrolysis/gasification of lignin over Ni–Ca–Al catalyst was investigated and filamentous carbon was produced.[24] Meanwhile, no evident carbon products can be found during the catalytic steam gasification of lignin over CaO.[25] This may be highly associated with the catalyst employed and operating conditions conducted.

Fig. 2 shows TEM images of the carbon materials-Ni/Al_2O_3 composites. It can be found that filamentous carbon derived from PE possessed a clearly tubular structure and relatively smooth surface, which is assigned to well-ordered CNTs (PE-CNTs-Ni/Al_2O_3). The diameter of the CNTs is in the range of 10–100 nm and the length is over 10 μm. This is well coincided with the SEM result (Fig. 1a and b). However, in addition to a small amount of well-ordered CNTs in a tubular structure, the filamentous carbon from PE/LG mixture appears to be mainly made up of highly curved cone-shape CNTs (PE/LG-CNTs-Ni/Al_2O_3) (Fig. 2c and d). The diameter and length of the curved cone-shape CNTs are in the range of about 10–100 nm and about 0.1–1 μm, respectively, which is consistent with the SEM result in Fig. 1c and d. Compared to the well-ordered CNTs from catalytic reforming of PE, the highly curved cone-shape CNTs from PE/LG mixture may reveal that the involvement of LG results in the occurrence of abundant structure defects. Moreover, the CNTs in PE-CNTs-Ni/Al_2O_3 with hollow tip can be easily seen in Fig. 2a and b further shows that the top end of the CNTs encapsulates a metallic particle in a diameter of 12 nm, indicating that the growth of the CNTs from catalytic reforming PE follows the tip-growth model.[26] Similar growth model may be responsible for the growth of curved cone-shape CNTs from catalytic reforming the mixture of PE and LG according to the TEM results in Fig. 2c and d due to hollow tip and encapsulated metal particle can be found as well. Fig. 2e and f reveals that the carbon materials derived from catalytic reforming LG (LG-Chars-Ni/Al_2O_3) are mainly composed of amorphous carbon.

XRD patterns of carbon materials-Ni/Al_2O_3 composites are presented in Fig. 3a. In addition to several pronounced characteristic peaks of Al_2O_3 and Ni, a small diffraction peak at $2\theta =$

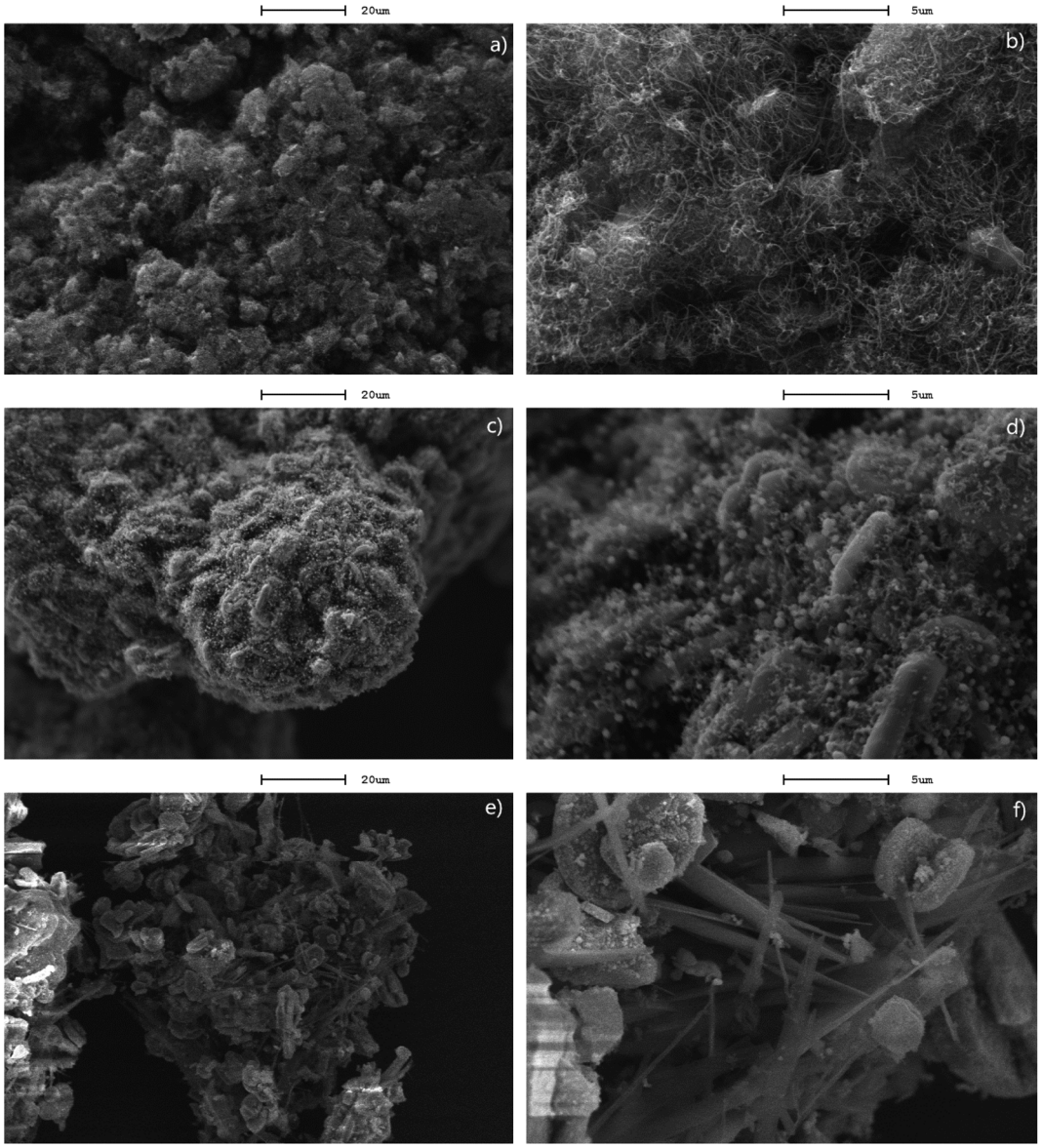

Fig. 1 SEM images of carbon materials-Ni/Al_2O_3 composites derived from different carbon sources using Ni/Al_2O_3 as catalyst, (a and b) PE; (c and d) PE/LG mixture; (e and f) LG.

26.5° in PE-CNTs-Ni/Al_2O_3 and PE/LG-CNTs-Ni/Al_2O_3 corresponding to the plane (002) of graphite like structure also can be observed, whereas the peak can not be found in LG-Chars-Ni/Al_2O_3.[27] This result reveals that the carbon materials from PE and PE/LG mixture contain a large amount of relatively well-ordered carbon in graphitic nature, while amorphous carbon is mainly responsible for the carbon material from LG, which is well in agreement with the SEM and TEM results. Fig. 3b shows TG curves of carbon materials-Ni/Al_2O_3 composites under air atmosphere from ambient temperature to 850 °C. It can be seen that PE-CNTs-Ni/Al_2O_3 exhibits good thermal stability before 355 °C with negligible weight loss. After that, PE-CNTs-Ni/Al_2O_3 undergoes a weight increase stage taking place at 355–516 °C, followed by a weight loss stage in the range of 516–682 °C. The weight increase stage can be attributed to the oxidation of Ni particle (from Ni to NiO) in PE-CNTs-Ni/Al_2O_3, which is originated from the reduction of catalyst precursor (NiO) by the pyrolysis intermediates of PE, such as ethylene. While the weight loss stage is related to the oxidation of CNTs. Similarly, the weight change of LG/PE-CNTs-Ni/Al_2O_3 exhibits a similar trend with that of PE-CNTs-Ni/Al_2O_3. The main difference lies in the initial temperatures of the weight increase and weight decrease of PE/LG-CNTs-Ni/Al_2O_3, which is 291 and 482 °C, respectively, both lowering than those of PE-CNTs-Ni/Al_2O_3. According to the TEM analysis, this result may result from the presence of abundant structure defects in PE/LG-CNTs-Ni/Al_2O_3. For LG-Chars-Ni/Al_2O_3, a successive weight loss stage can be seen at the whole temperature range, which indicates that the content of chars (amorphous carbon) in LG-Chars-Ni/Al_2O_3 is relatively high and the chars possess a relatively low thermal

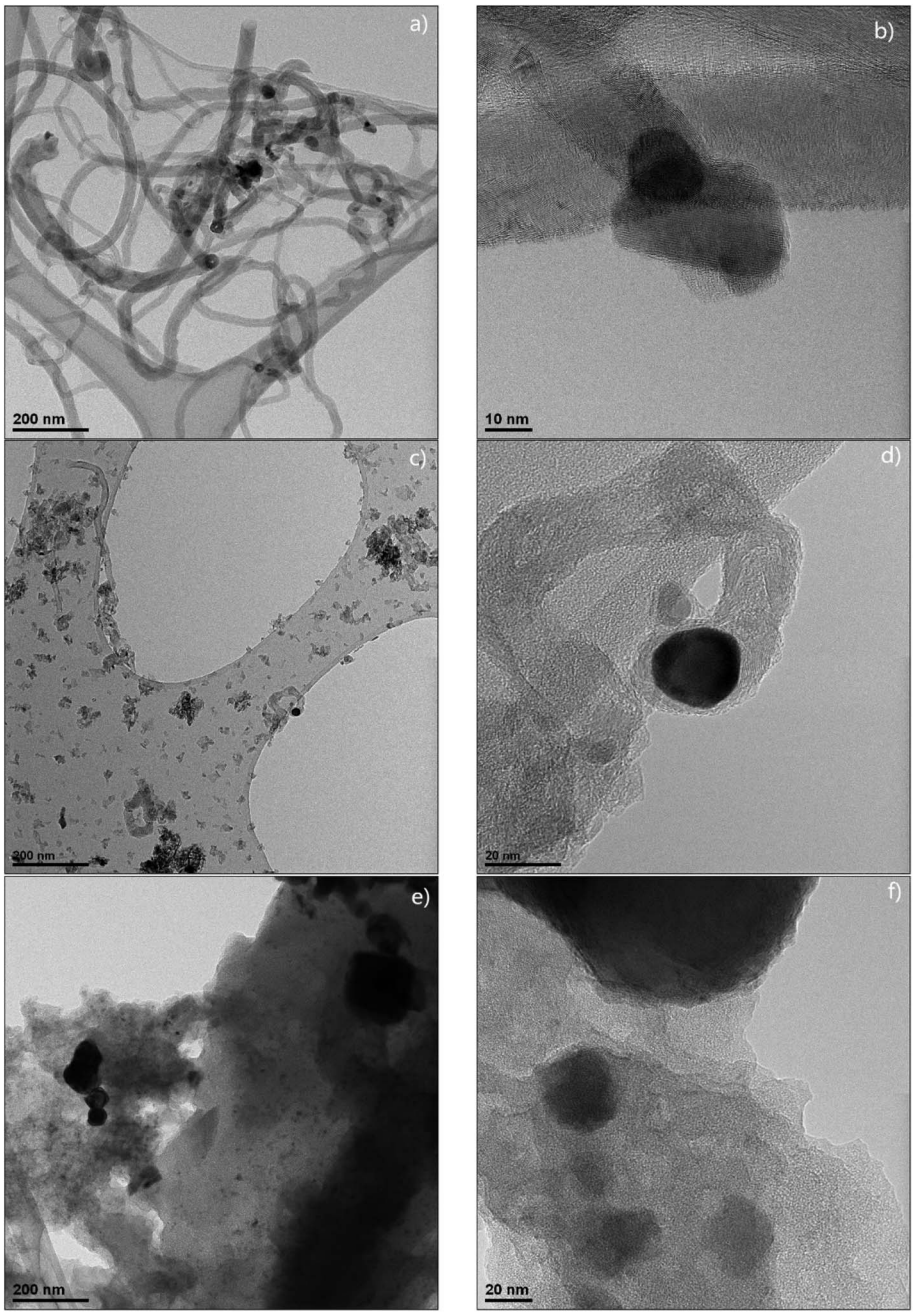

Fig. 2 TEM images of carbon materials-Ni/Al_2O_3 derived from different carbon sources, (a and b) PE; (c and d) PE/LG; (e and f) LG.

stability. Furthermore, the high solid residue ranging from 85.2% to 97.4% for the three composites is mainly assigned to the presence of the mixture of Al_2O_3 and NiO (see Table 1).

The surface functional groups of carbon materials-Ni/Al_2O_3 composites were analyzed by FT-IR, and the results are presented in Fig. 4. The strong adsorption bands between 630 and 700 cm^{-1} correspond to the stretching vibration of Al–O bond originating from catalyst substrate (Al_2O_3), which can be evidently found in all carbon materials-Ni/Al_2O_3 composites.[28] O-containing surface functional groups, such as C=O occurring at the adsorption bands at the range of 1044–1110 cm^{-1}, C–O observing at the adsorption band at 1430 cm^{-1}, and –OH presenting at the adsorption bands between 3200–3300 cm^{-1}, can be only found in PE/LG-CNTs-Ni/Al_2O_3 and LG-Chars-Ni/Al_2O_3 thanks to the presence of a large amount of O content in LG.[29] On the other hand, the band at 1500 cm^{-1} attributing to aromatic C=C are only seen in PE-CNTs-Ni/Al_2O_3 and PE/LG-CNTs-Ni/Al_2O_3, which may be related to the graphitic structure in CNTs.

Physicochemical characteristics of carbon materials-Ni/Al_2O_3 composites are shown in Table 1. The carbon yield of the three types of composites follows an order of PE-CNTs-Ni/Al_2O_3 < PE/LG-CNTs-Ni/Al_2O_3 < LG-Chars-Ni/Al_2O_3, which is well coincided with the TG result in Fig. 3b. The proximate analysis

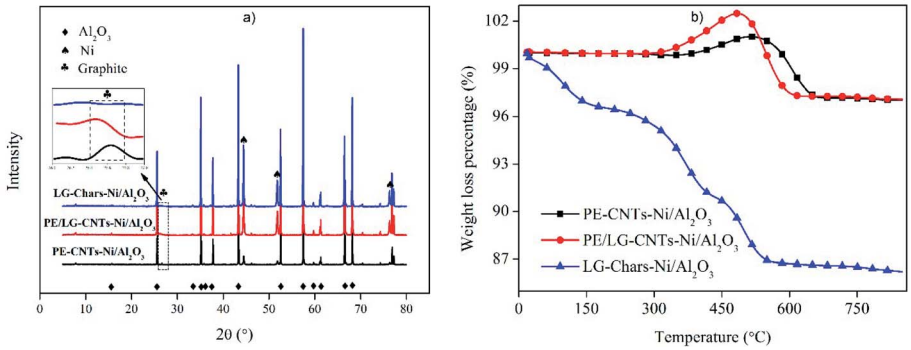

Fig. 3 XRD patterns (a) and TPO (b) of carbon materials-Ni/Al_2O_3 composites.

reveals that fixed carbon is the main content in PE-CNTs-Ni/Al_2O_3 and PE/LG-CNTs-Ni/Al_2O_3 while the volatile matter (7.3%) in LG-Chars-Ni/Al_2O_3 is nearly equivalent to that of the fixed carbon (7.8%) except for ash content. The higher content of volatile matter in LG-Chars-Ni/Al_2O_3 highly relates to its inner amorphous carbon structure, leading to lower thermal stability.[30] PE-CNTs-Ni/Al_2O_3 is mainly composed of C and H according to ultimate analysis. For PE/LG-CNTs-Ni/Al_2O_3 and LG-Chars-Ni/Al_2O_3, a certain amount of O and S can be detected besides C and H. The presence of O content may be highly related to the O-containing surface functional groups in PE/LG-CNTs-Ni/Al_2O_3 and LG-Chars-Ni/Al_2O_3 as shown in Fig. 4. PE-CNTs-Ni/Al_2O_3 and PE/LG-CNTs-Ni/Al_2O_3 is similar in pore characteristics involving surface area (48.87–52.12 $m^2\ g^{-1}$), total pore volume (0.15–0.16 $cm^3\ g^{-1}$) and average pore diameter (10.8–13.5 nm). By comparison, LG-Chars-Ni/Al_2O_3 possesses relatively inferior surface area (2.61 $m^2\ g^{-1}$) and total pore volume (0.02 $cm^3\ g^{-1}$). It is reported that the relatively higher O content in biomass (25–45%) causes the extensive polycondensation of the intermediates during pyrolysis, which is not beneficial to produce porous material.[29] The pH_{pzc} of PE-CNTs-Ni/Al_2O_3 is 8.16 while that of PE/LG-CNTs-Ni/Al_2O_3 decreases to 5.42 due to the introduction of LG, which brings into a large amount of O-containing surface functional groups.[31]

In order to understand the growth mechanism of the carbon materials prepared from different carbonaceous precursors (*i.e.*, PE, LG and their mixture), the volatile components of the carbonaceous precursors are determined using Py-GC/MS and the corresponding analysis is shown in Fig. 5. It can be found that the volatiles of PE mainly consists of a large amount of alkanes (i.g., heptane, octane, nonane, tetradecane, pentadecane, hexadecane, heptadecane, octadecane) and alkenes (i.g., propylene, butene, cyclopentene, heptene, nonadecene, decene, pentadecane, cetene), as well as a small amount of aromatic hydrocarbons, which is well in agreement with previous study.[32] By comparison, oxygenated compounds including phenols (i.g., phenol, cresol, catechol), aromatic aldehydes (i.g., benzaldehyde), aromatic alcohols (i.g., benzenediol) and aromatic

Table 1 Proximate analysis, ultimate analysis and other properties of carbon materials-Ni/Al_2O_3 composites

	PE-CNTs-Ni/Al_2O_3	PE/LG-CNTs-Ni/Al_2O_3	LG-Chars-Ni/Al_2O_3
Yield	4.71	6.98	18.42
Proximate analysis			
Fixed carbon (%)	4.1	4.8	7.6
Volatile matter (%)	0.1	0.8	7.3
Ash (%)	95.8	94.4	85.1
Ultimate analysis			
C (%)	4.34	4.84	6.53
H (%)	0.01	0.18	0.45
O (%)	—	0.68	1.85
S (%)	—	0.06	0.28
Other properties			
SSA ($m^2\ g^{-1}$)	48.87	52.13	2.61
TPV ($cm^3\ g^{-1}$)	0.15	0.16	0.02
APD (nm)	10.8	13.5	1.6
Solid reside[a]	97.3%	97.4%	85.2%
pHpzc	8.16	5.42	5.28

[a] The mass remaining after TPO analysis.

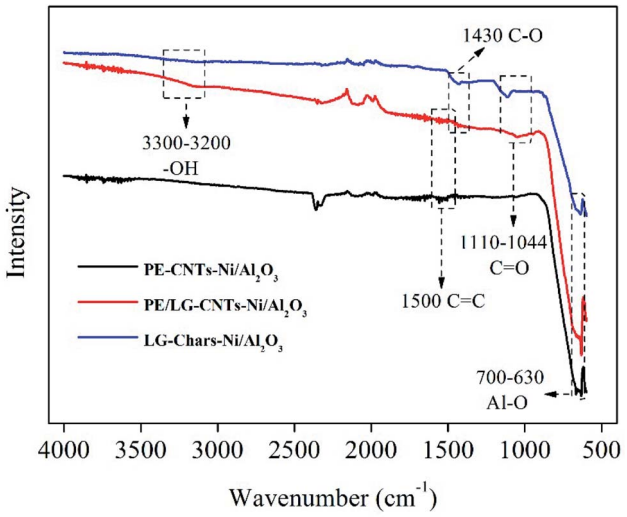

Fig. 4 FTIR spectra of carbon materials-Ni/Al_2O_3 composites.

ketones (i.e., methoxyacetophenone) are the main components of the volatiles of LG. Jin *et al.* obtained similar results as black liquor-derived LG were carried out to pyrolyze.[33] Interestingly, the types of hydrocarbons and oxygenated compounds in the volatiles obtained from the pyrolysis of PE together with LG are evidently reduced in comparison with the pyrolysis products from PE alone and LG alone. Moreover, a certain amount of newly produced substances, such as toluene, can be found, which can be attributed to the interaction between the pyrolysis intermediates of PE and LG, such as hydrodeoxygenation and anti polycondensation.[33]

Alkanes, alkenes and aromatic hydrocarbons are considered the superior carbonaceous feedstocks for the preparation of carbon nanomaterials such as CNTs, carbon nanofibres, and graphene *via* catalytic reforming.[34] While the catalytic reforming of phenols, aromatic aldehydes, aromatic alcohols and aromatic ketones only can produce amorphous carbon due to their complex structure and high oxygen content.[35] Accordingly, well-ordered CNTs can be obtained from the catalytic reforming of the pyrolysis products from PE while amorphous carbon is the main component of the solid carbon product from LG. This has been well confirmed by TEM, XRD and TG results. The volatiles from the co-pyrolysis of PE and LG are mixtures mainly consisting of hydrocarbons and oxygenated compounds. It is reported that oxygenated compounds, such as phenol like compounds, can be employed to produce CNTs with abundant defects and O-containing surface functional groups in the presence of reductant (H_2 or hydrocarbons).[36] This may be the main reason for the curved cone-shape CNTs produced from the catalytic reforming of PE/LG, which is well coincided with the TEM and FT-IR results. According to the results of SEM, TEM, XRD, TG and FTIR, possible mechanisms of the growth of carbon materials over the Ni/Al_2O_3 catalysts varying from the raw materials are proposed (see Scheme 1).

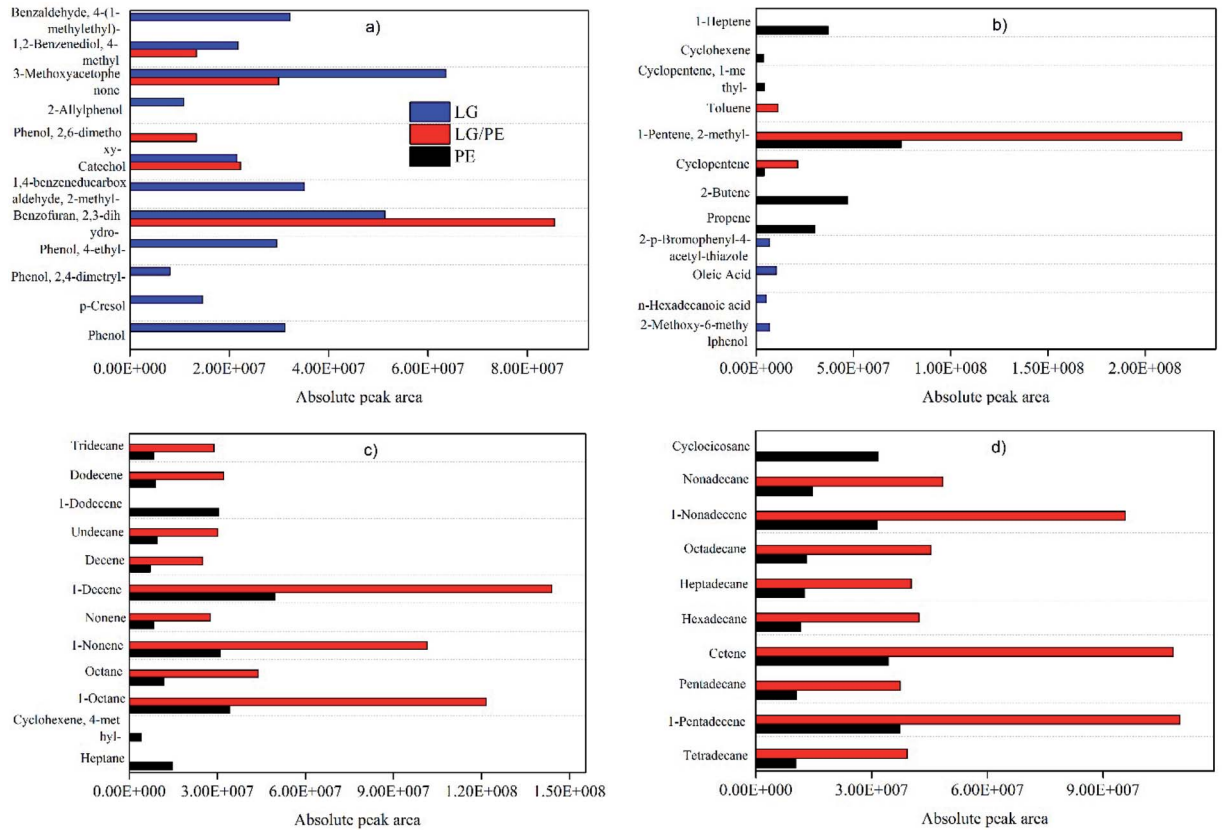

Fig. 5 Volatile products of PE, LG and their mixture (PE/LG) as determined by Py-GC/MS.

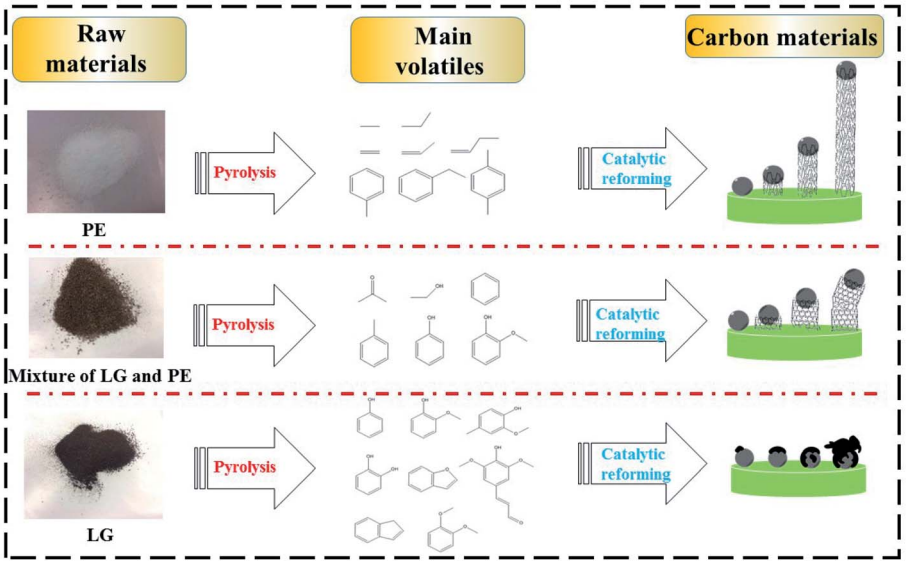

Scheme 1 Possible growth mechanism of different types of carbon materials.

3.2 Adsorption capability towards Pb(II)

3.2.1 Effect of initial concentration and isotherm analysis. Fig. 6 depicts the adsorption capability of Pb(II) onto the three types of carbon materials-Ni/Al_2O_3 composites (*i.e.*, PE-CNTs-Ni/Al_2O_3, PE/LG-CNTs-Ni/Al_2O_3 and LG-Chars-Ni/Al_2O_3) influenced by various initial concentrations of Pb(II) (20–400 mg L^{-1}). Overall, there is a roughly positive relationship between Pb(II) initial concentration and corresponding adsorption capability in certain Pb(II) initial concentration range, *i.e.*, the increase of Pb(II) initial concentration could promote the enhancement of the adsorption capability of the three types of composites towards Pb(II). Particularly, the adsorption capacity of Pb(II) using the composites are obviously increased with the increase of Pb(II) initial concentration in the range of 20–150 mg L^{-1}, where a linear correlation with correlation coefficients (R^2) of 0.96–0.98 between Pb(II) initial concentration and adsorption capacity can be observed. The increase of Pb(II) adsorption capacity is gradually slowed down as the Pb(II) initial concentration is over 150 mg L^{-1}. A stronger driving force between Pb(II) and the composite surface under a higher Pb(II) initial concentration may be responsible for the increase of Pb(II) adsorption capacity with the increase of Pb(II) initial concentration. While the gradual saturation of the adsorption vacancies of the composites with the increase of the initial concentration to 150–400 mg g^{-1} results in the slow increase of adsorption capacity.[2] The maximum adsorption capacity of PE-CNTs-Ni/Al_2O_3 towards Pb(II) is 28.71 mg g^{-1} at the Pb(II) initial concentration of 400 mg L^{-1}, which is comparable with those of some waste-based adsorbents.[37] The excellent adsorption capacity toward Pb(II) of PE-CNTs-Ni/Al_2O_3 may relate to the presence of CNTs and Al_2O_3. LG-Chars-Ni/Al_2O_3 shows a slightly better adsorption capacity towards Pb(II) in comparison with PE-CNTs-Ni/Al_2O_3 in the whole Pb(II) initial concentration range (20–400 mg L^{-1}). According to the physicochemical properties results presented above, it is inferred that amorphous carbon with abundant O-containing surface

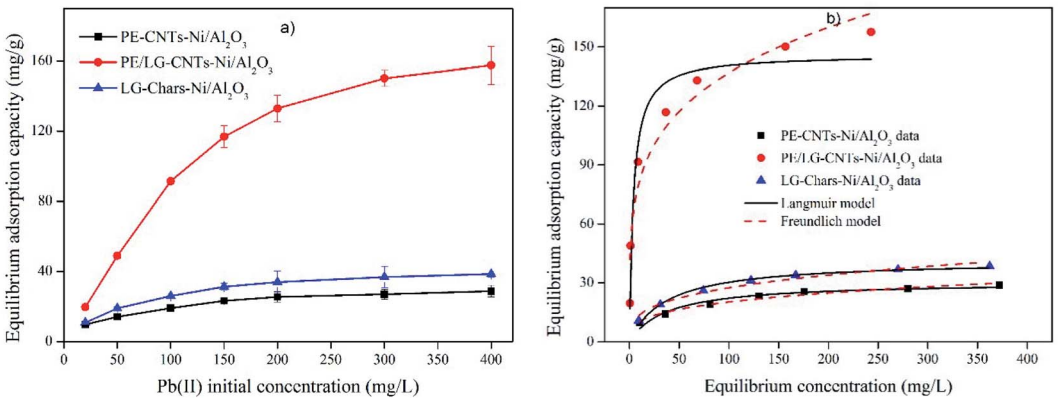

Fig. 6 Effect of Pb(II) initial concentration on the adsorption of Pb(II) on PE-CNTs-Ni/Al_2O_3, PE/LG-CNTs-Ni/Al_2O_3 and LG-Chars-Ni/Al_2O_3 composites (a) and isotherm fitting using Langmuir and Freundlich models (b).

functional groups in LG-Chars-Ni/Al_2O_3 may play an key role in Pb(II) removal. It is worth noting that LG/PE-CNTs-Ni/Al_2O_3 shows a superior adsorption capability towards Pb(II) in comparison with PE-CNTs-Ni/Al_2O_3 and LG-Chars-Ni/Al_2O_3, whose adsorption capacity are 2–5.5 and 1.8–4 folds of those using PE-CNTs-Ni/Al_2O_3 and LG-Chars-Ni/Al_2O_3, respectively. This result reveals that the presence of nanostructure (CNTs) and O-containing surface functional groups are greatly favorable to enhance the adsorption capability of composite towards Pb(II).

In order to clarify the relationship between the Pb(II) concentration adsorbed on composite surface and remained in solution at adsorption equilibrium, two typical adsorption isotherm models, *i.e.*, Langmuir model (eqn (1)) and Freundlich model (eqn (2)) are employed to fit the adsorption processes. Langmuir model is applicable on the assumption of monolayer adsorption of adsorbate molecular onto a homogeneous adsorbent surface with no interactions between the adsorbed molecules. Freundlich model assumes that the adsorption enthalpy on the sorbent surface is heterogeneously distributed and increased with a surface coverage of adsorbent.

$$q_e = \frac{Q_m K_l C_e}{1 + K_l C_e} \quad (1)$$

$$q_e = K_f C_e^{\,n} \quad (2)$$

where q_e is the equilibrium Pb(II) adsorption capacity (mg g^{-1}), Q_m is the maximum capacity (mg g^{-1}), K_l is the Langmuir binding term related to interaction energies (L mg^{-1}), C_e is the equilibrium concentration of Pb(II) (mg L^{-1}), n is the Freundlich linearity constant, K_f represents the Freundlich affinity coefficient ($mg^{(1-n)}$ L^n g^{-1}).

The fitting results for Pb(II) adsorption using Langmuir and Freundlich models are shown in Fig. 6b and Table 2. It is found that the R^2 values of PE-CNTs-Ni/Al_2O_3, PE/LG-CNTs-CNTs-Ni/Al_2O_3 and LG-Chars-Ni/Al_2O_3 composites from Langmuir model are 0.97, 0.96 and 0.99, respectively, which are slight higher than those from Freundlich model (0.94–0.95), indicating that the adsorption processes could be well described by Langmuir model and the adoption of Pb(II) onto the three composites is subjected to a homogeneous monolayer adsorption. Similar results have been reported when carbon nanotubes/$CoFe_2O_4$ magnetic hybrid material was employed as adsorbents to remove Pb(II).[38] The theoretical maximum adsorption capacity of Pb(II) (Q_m) calculated from Langmuir model are 30.47, 146.08 and 41.44 mg g^{-1} for PE-CNTs-Ni/Al_2O_3, PE/LG-CNTs-Ni/Al_2O_3 and LG-Chars-Ni/Al_2O_3 composites, respectively. PE/LG-CNTs-Ni/Al_2O_3 composite shows the highest Q_m value among the three composites employed, which is about 4.8 and 3.5 folds to those of PE-CNTs-Ni/Al_2O_3 and LG-Chars-Ni/Al_2O_3 composites, respectively, revealing that PE/LG-CNTs-Ni/Al_2O_3 composite has a superior adsorption capability to Pb(II). Moreover, the Q_m of PE/LG-CNTs-Ni/Al_2O_3 composite is much higher than most of the adsorption in previous reports as shown in Table S3.† For example, the adsorbed Pb(II) on PE/LG-CNTs-Ni/Al_2O_3 composite is about 3 folds higher than those of CNTs/bagasse composite (56.6 mg g^{-1}) and CNTs@zeolite composite (55.74 mg g^{-1}).[39,40] On the other hand, K_l, the Langmuir bonding term related to interaction energies, can be employed to analyze the bonding strength between adsorbate molecular and the adsorption sites of adsorbent. According to the results in Table 2, the K_l values of the three composites are subject to an order of PE-CNTs-Ni/Al_2O_3 (0.02 L g^{-1}) < LG-Chars-Ni/Al_2O_3 (0.03 L g^{-1}) < PE/LG-CNTs-Ni/Al_2O_3 (0.26 L g^{-1}), which is consistent with the trend of Q_m. This suggests that among the three composites, PE/LG-CNTs-Ni/Al_2O_3 possesses not only the highest Q_m value but also the strongest bonding strength towards Pb(II).

The affinities between Pb(II) and composite can be further predicted by K_l using a dimensionless separation factor R_L according to the following equation (eqn (3)):

$$R_L = \frac{1}{1 + K_l C_o} \quad (3)$$

where K_l is a fitted parameter of Langmuir model, C_o is the highest initial Pb(II) concentration in solution (mg L^{-1}).

It is reported that $R_L > 1$, $R_L = 1$, $1 > R_L > 0$ and $R_L = 0$ indicates the isotherm to be unfavorable, linear, favorable and irreversible, respectively.[41] The calculated values of PE-CNTs-Ni/Al_2O_3, PE/LG-CNTs-CNTs-Ni/Al_2O_3 and LG-Chars-Ni/Al_2O_3 composites are 0.11–0.71, 0.01–0.16 and 0.08–0.63, respectively, suggesting that the adsorption of Pb(II) onto the three composites are favorable.

Table 2 Isotherm parameters of Pb(II) adsorption by different composites derived from Langmuir and Freundlich models

	PE-CNTs-Ni/Al_2O_3	PE/LG-CNTs-Ni/Al_2O_3	LG-Chars-Ni/Al_2O_3
Langmuir			
Q_m (mg g^{-1})	30.47	146.08	41.44
K_l (L mg^{-1})	0.02	0.26	0.03
R^2	0.97	0.96	0.99
Freundlich			
K_f ($mg^{(1-n)}$ L^n g^{-1})	5.15	48.67	6.73
n	3.37	4.45	3.28
R^2	0.95	0.94	0.94

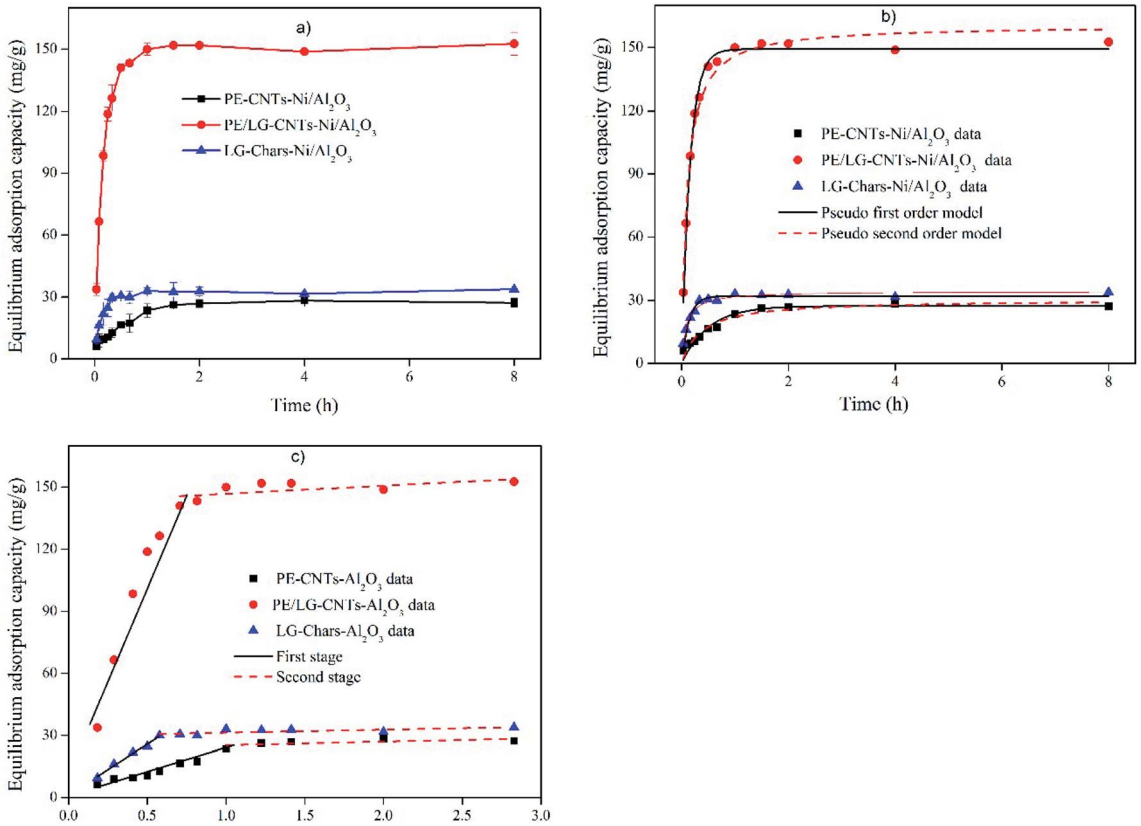

Fig. 7 Effect of contact time on the adsorption of Pb(II) on PE-CNTs-Ni/Al_2O_3, PE/LG-CNTs-Ni/Al_2O_3 and LG-Chars-Ni/Al_2O_3 composites (a), kinetic fitting using Pseudo-first-order and Pseudo-second-order models (b) and Weber–Morris model (c).

3.2.2 Effect of contact time and kinetic analysis. The effect of contact time on the adsorption of Pb(II) on PE-CNTs-Ni/Al_2O_3, PE/LG-CNTs-Ni/Al_2O_3 and LG-Chars-Ni/Al_2O_3 composites in the range of 0–8 h is shown in Fig. 7. It can be found that the adsorption of Pb(II) on the three composites fast proceeds with the initial 1 h, which accounts for 86.24–98.23% of the adsorption capacity at equilibrium. The adsorption rate of PE-CNTs-Ni/Al_2O_3, PE/LG-CNTs-Ni/Al_2O_3 and LG-Chars-Ni/Al_2O_3 composites at this stage are up to 23.5, 149.9 and 33.0 mg (g^{-1} h^{-1}), respectively. Afterwards, the adsorption of Pb(II) gradually is slowed down with the increase of contact time and roughly reaches equilibrium in 2 h. The high adsorption rate in initial contact time can be attributed to the presence of adequate vacant adsorption sites on the surface of composites while the gradual consumption of active sites results in a difficulty in the adsorption of Pb(II).[2]

The interaction between Pb(II) and the surface adsorption sites of composites with contact time can be investigated by adsorption kinetics models. Two widely accepted kinetics models, *i.e.*, Pseudo-first-order (eqn (4)) and Pseudo-second-order (eqn (5)) models, are conducted to simulate the adsorption. Pseudo-first-order model considers the adsorption to a reversible reaction, while Pseudo-second-order model is associated with a chemisorption process.

$$\frac{dq_t}{d_t} = k_1(q_e - q_t) \quad (4)$$

$$\frac{dq_t}{d_t} = k_2(q_e - q_t)^2 \quad (5)$$

where q_e and q_t represent the amount of Pb(II) adsorbed at equilibrium and at time t, respectively (mg g^{-1}), t is the contact time (h), k_1 and k_2 are adsorption rate constants of the Pseudo-first-order (h^{-1}) and Pseudo-second-order (g (mg^{-1} h^{-1})) models, respectively.

The kinetics fitting results are exhibited in Fig. 7b and the obtaining fitting parameters are shown in Table 3. Pseudo-second-order model can well describe the adsorption of Pb(II) using the three composites with R^2 values in the range of 0.94–0.99, which are higher than those of Pseudo-first-order model (0.92–0.95). Moreover, the calculated equilibrium adsorption capacity (q_e) from Pseudo-second-order model are 28.35, 153.64 and 34.34 mg g^{-1} for PE-CNTs-Ni/Al_2O_3, PE/LG-CNTs-Ni/Al_2O_3 and LG-Chars-Ni/Al_2O_3 composites, respectively, which are much close to their experimental values (Q_{exp}). It is therefore demonstrated that Pseudo-second-order model is an ideal model to simulate the adsorption of Pb(II) using the three composites. Pseudo-second-order model is also found to be the best kinetic model to simulate the adsorption of Pb(II) using

Table 3 Kinetic parameters of Pb(II) adsorption by different carbon materials derived from Pseudo-first-order, Pseudo-second-order and Weber–Morris models

	PE-CNTs-Ni/Al_2O_3	PE/LG-CNTs-Ni/Al_2O_3	LG-Chars-Ni/Al_2O_3
Q_{exp} (mg g^{-1})	28.25	152.60	34.80
Pseudo-first-order model			
K_1 (h^{-1})	1.98	6.46	7.36
q_e (mg g^{-1})	27.31	143.24	32.06
R^2	0.92	0.95	0.94
Pseudo-second-order model			
K_2 (g mg h^{-1})	0.09	0.06	0.34
q_e (mg g^{-1})	28.35	153.64	34.34
R^2	0.94	0.99	0.98
Weber-Morris model			
First stage			
a_1 [a]	13.14	268.45	49.34
b_1 [b]	4.26	−13.26	1.10
R^2	0.90	0.99	0.99
Second stage			
a_2	22.02	61.98	6.74
b_2	0.08	91.19	25.60
R^2	0.97	0.92	0.90
Third stage			
a_3	0.63	0.58	0.36
b_3	25.97	150.02	32.13
R^2	0.91	0.91	0.91

[a] Slope. [b] Intercept.

carbon nanotubes/$CoFe_2O_4$ magnetic hybrid material as reported in the study from Zhou *et al.*[38] Moreover, the adsorption well following Pseudo-second-order model reveals that the adsorption of Pb(II) using the three composites are mainly dominated by a series of chemical reactions.

Weber–Morris model analysis is usually carried out to interpret the mass transfer and intraparticle diffusion mechanism between the adsorbate and the adsorbent during adsorption process, which can be expressed by the following equation (eqn (6)).

$$q_t = a \times t^{0.5} + b \quad (6)$$

where q_t is the adsorption capacity at contact time t (mg g^{-1}), a is the intraparticle rate constant (slope), b is the intercept, t is contact time (h).

The relationship between the adsorption capacity of Pb(II) at contact time t (q_t) and the square root of corresponding contact time is plotted in Fig. 7c and the obtained parameters is presented in Table 3. As shown, the adsorption of Pb(II) using the three composites can be well divided into three linear lines with different slopes (R^2 = 0.90–0.99). It is well-established that the first linear stage is assigned to the mass transfer of Pb(II) from the bulk solution to the surface of composite, while the second and third stages are attributed to intraparticle diffusion of Pb(II) into the porous interior structure of composite. It is found that the slopes of the first linear stage from the three composites are 13.14–268.45 which are steeper than those of the second and third stages (0.36–61.98) (except for PE-CNTs-Ni/Al_2O_3). This observation indicates that the mass transfer of Pb(II) from the bulk solution to the surface of the composite is much fast and fierce, while the intraparticle diffusion is relatively slow and not the rate-limiting process for the adsorption.

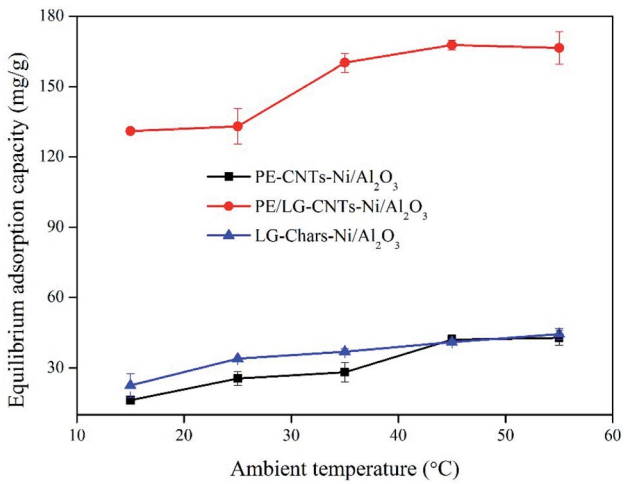

Fig. 8 Effect of ambient temperature on the adsorption of Pb(II) on PE-CNTs-Ni/Al_2O_3, PE/LG-CNTs-Ni/Al_2O_3 and LG-Chars-Ni/Al_2O_3 composites.

3.2.3 Effect of ambient temperature and thermodynamic analysis. The effect of ambient temperature ranging from 15 to 45 °C on the adsorption of Pb(II) on PE-CNTs-Ni/Al_2O_3, PE/LG-CNTs-Ni/Al_2O_3 and LG-Chars-Ni/Al_2O_3 composites is investigated and the results are shown in Fig. 8. It can be seen that the increase of ambient temperature generally causes an increase in the adsorption capacity of Pb(II) using the three composites. In detail, the adsorption capacity of Pb(II) is increased from 16.2 to 42.9 mg g^{-1} for PE-CNTs-Ni/Al_2O_3, 131.05 to 166.45 mg g^{-1} for PE/LG-CNTs-Ni/Al_2O_3 and 22.47 to 44.45 mg g^{-1} for LG-Chars-Ni/Al_2O_3, respectively, as the ambient temperature elevates from 15 to 45 °C. The increase of adsorption capacity with the increase of ambient temperature suggests that the adsorption of Pb(II) on the composite is dominated by an endothermic nature. Similar findings have been found in previous reports.[42] It is reported that ambient temperature determines the random motion of adsorbate and the combination or fracture of chemical bonds between adsorbate and the surface adsorption sites of adsorbent.[2] A high ambient temperature can provide Pb(II) sufficient energy to overcome the resistance of the hydrated ion layer and get to the interior matrix of the composite to interact with the active adsorption sites.

The thermodynamic parameters, involving Gibbs free energy (ΔG^0), enthalpy (ΔH^0) and entropy (ΔS^0), are generally employed to reveal the deep relationship between the ambient temperature and the adsorption of Pb(II), which can be obtained from a series of equations (eqn (7)–(9)). ΔG^0 represents an indication of the spontaneity of a chemical reaction. Particularly, ΔG^0 in a negative value reveals a spontaneous reaction, while an unspontaneous reaction would lead to a positive value of ΔG^0. ΔH^0 and ΔS^0 are associated with the energy change of system and the randomness state of the adsorption, respectively.

$$\Delta G^0 = RT \ln K_e \quad (7)$$

$$K_e = \frac{q_e}{C_e} \quad (8)$$

$$\ln K_e = \frac{\Delta H^0}{RT} + \frac{\Delta S^0}{R} \quad (9)$$

where R is gas constant (8.314 J (mol^{-1} K^{-1})), T is the absolute temperature (K), q_e is Pb(II) concentration on the composite at equilibrium (mg g^{-1}), C_e is the remaining Pb(II) concentration in the solution at equilibrium (mg L^{-1}), ΔG^0 (kJ mol^{-1}), ΔH^0 (kJ mol^{-1}) and ΔS^0 (J (mol^{-1} K^{-1})) can be calculated from the slope and intercept of the plot of ΔG^0 *versus* T.

The calculated thermodynamic parameters of the adsorption of Pb(II) on PE-CNTs-Ni/Al_2O_3, PE/LG-CNTs-Ni/Al_2O_3 and LG-Chars-Ni/Al_2O_3 composites are presented in Table 4. It can be found that the values of ΔG^0 obtained from the adsorption of Pb(II) using the three composites under various temperatures are negative (−6.94∼−18.82 kJ mol^{-1}), revealing that the adsorption can proceed spontaneously. The absolute values of ΔG^0 for each composite shows a positive relationship with the ambient temperature, which indicates that the increase in ambient temperature is favorable for the adsorption. The ΔH^0 values of PE-CNTs-Ni/Al_2O_3, PE/LG-CNTs-Ni/Al_2O_3 and LG-Chars-Ni/Al_2O_3 composites for Pb(II) adsorption are 22.61, 22.30 and 14.78 kJ mol^{-1}, respectively, indicating that the adsorption are subjected to be endothermic. In other words, an increase in ambient temperature are beneficial to the adsorption of Pb(II) using the composites. This well coincides with the result in Fig. 8. Moreover, the positive values of ΔS^0 suggests a fierce randomness state between the interface of composite and Pb(II) solution during Pb(II) adsorption.

3.2.4 Effect of solution pH. Solution pH significantly affects the surface charges, the degree of ionization of the adsorbent and the speciation of metal ions, hence playing an important role in the adsorption of heavy metal ions.[2] In order to eliminate the formation of soluble hydroxyl complexes or precipitates, the effect of solution pH on the adsorption of Pb(II) on PE-CNTs-Ni/Al_2O_3, PE/LG-CNTs-Ni/Al_2O_3 and LG-Chars-Ni/Al_2O_3 composites is conducted in the pH range of 2–6, and the result is given in Fig. 9. As depicts, the adsorption of Pb(II) in various solution pH are dramatically different from the types of

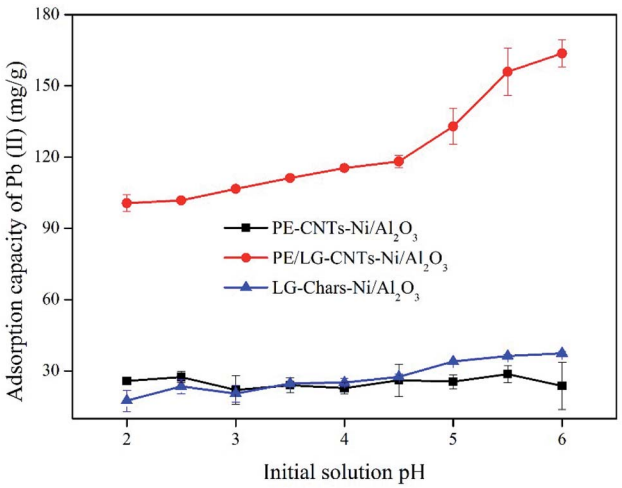

Fig. 9 Effect of solution pH on the adsorption of Pb(II) on PE-CNTs-Ni/Al_2O_3, PE/LG-CNTs-Ni/Al_2O_3 and LG-Chars-Ni/Al_2O_3 composites.

Table 4 Thermodynamic parameters of Pb(II) adsorption by different composites

	ΔG^0 (kJ mol^{-1})					ΔH^0 (kJ mol^{-1})	ΔS^0 (J (mol^{-1} K^{-1}))
	288 (K)	298 (K)	308 (K)	318 (K)	328 (K)		
PE-CNTs-Ni/Al_2O_3	−6.94	−8.45	−9.01	−10.58	−10.98	22.61	100.93
PE/LG-CNTs-Ni/Al_2O_3	−14.27	−14.87	−17.14	−18.36	−18.82	22.30	126.62
LG-Chars-Ni/Al_2O_3	−7.80	−9.26	−9.84	−10.50	−11.11	14.78	79.50

the composites. The adsorption of Pb(II) using PE-CNTs-Ni/Al_2O_3 composite slightly fluctuates with solution pH with an adsorption capacity range of 6.7 mg L^{-1} (the difference between the maximum and minimum adsorption capacity), indicating that solution pH has a slight influence on the adsorption. By comparison, the adsorption of Pb(II) by PE/LG-CNTs-Ni/Al_2O_3 and LG-Chars-Ni/Al_2O_3 composites generally shows a positively pH-dependent trend, which is enhanced with the increase of solution. The adsorption capacity of Pb(II) using PE/LG-CNTs-Ni/Al_2O_3 and LG-Chars-Ni/Al_2O_3 composites are increased from 100.67 and 17.48 mg g^{-1} at the initial solution pH of 2 to 163.68 and 37.37 mg g^{-1} at the initial solution pH of 6, respectively. Particularly, the adsorption of Pb(II) by PE/LG-CNTs-Ni/Al_2O_3 composite increases slowly possessing an adsorption capacity range of 10.25 mg g^{-1} with the increase of solution pH when the solution pH is below 3.5. While an evident increase in the adsorption with an adsorption capacity range of 52.48 mg g^{-1} can be observed at the pH range of 3.5–6. It is reported that Pb mainly exists as Pb(II) when the solution pH is in the range of 1–6. Severe compete between the Pb(II) and H^+ will occur with the decrease of solution pH due to the increase of H^+ concentration. The high concentration of H^+ has a strong affinity to the complexation and ion exchange sites, especially for the O-containing surface functional groups in comparison with Pb(II).[7] Moreover, the H^+ in solution would cause the protonation of the composites, resulting in electrostatic repulsion between Pb(II) and the protonated surface of composites, which is not favorable for the adsorption of Pb(II).

3.2.5 Possible adsorption mechanisms. It is well-established that the physicochemical properties of adsorbent play vital roles in its adsorption performance and capability to contaminants.[43] According to the results from TEM, SEM, XRD, TG, FT-IR and other methods in the present study, a series of evident differences in physicochemical properties, such as the types of carbon materials (*i.e.*, well-order CNTs, curved cone-shape CNTs or amorphous carbon), pore structure (SSA, TPV and APD) and the surface chemistry properties of the composites can be found among PE-CNTs-Ni/Al_2O_3, PE/LG-CNTs-Ni/Al_2O_3 and LG-Chars-Ni/Al_2O_3 composites, which hence result in the great differences in the adsorption to Pb(II). Among PE-CNTs-Ni/Al_2O_3, PE/LG-CNTs-Ni/Al_2O_3 and LG-Chars-Ni/Al_2O_3 composites, PE/LG-CNTs-Ni/Al_2O_3 composite shows a fabulous adsorption to Pb(II), and the theoretical maximum adsorption capacity is about 4.8 and 3.5 folds to those of PE-CNTs-Ni/Al_2O_3 and LG-Chars-Ni/Al_2O_3 composites, respectively (see Table 2). Particularly, PE/LG-CNTs-Ni/Al_2O_3 present similar SSA and TPV values (see Table 1) with PE-CNTs-Ni/Al_2O_3 while the adsorption capacity are quite different, which may reveal that the adsorption mechanisms between the two composites are not dominated by pore-filling and would be great different. The possible mechanisms for the adsorption of Pb(II) on PE/LG-CNTs-Ni/Al_2O_3 composite analyzed according to its physicochemical properties are summarized as follows as depicted in Scheme 2: (1) complexation with O-containing surface functional groups. It is reported that the abundant O-containing surface functional groups, such as C=O, C–O, C–O–C, –OH, possess a strong affinity to Pb(II) and can greatly facilitate the adsorption of Pb(II) on carbon materials *via* complexation based on eqn (10)–(12).[43] A quantitative calculation on the adsorption of Pb(II) using peanut shell-based carbon material shows that 11.4% of the adsorbed Pb(II) can be attributed to the O-containing surface functional groups.[44] According to FT-IR analysis in Fig. 4, PE/LG-CNTs-Ni/Al_2O_3 composite has a large amount of C=O, C–O, –OH, suggesting that the complexation between Pb(II) and O-containing surface functional groups may make contributions to the adsorption of Pb(II). (2) Electrostatic attraction. The pHpzc value of PE/LG-CNTs-Ni/Al_2O_3 composite is 5.42 as shown in Table 1. According to the characteristics of pHpzc, the surface of PE/LG-CNTs-Ni/Al_2O_3 composite would be negatively charged as the solution pH is higher than 5.42. The adsorption

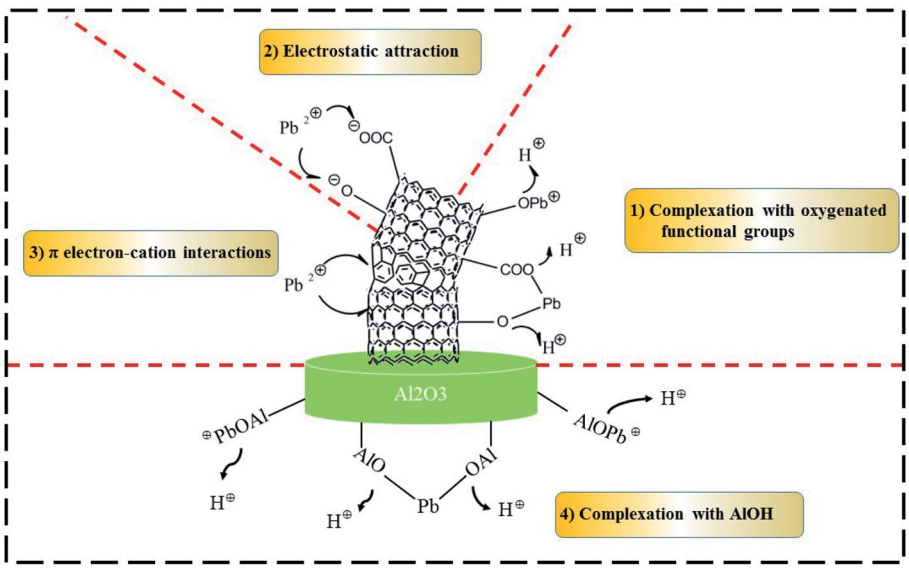

Scheme 2 The potential mechanisms for the adsorption of Pb(II) using PE/LG-CNTs-Ni/Al_2O_3 composite.

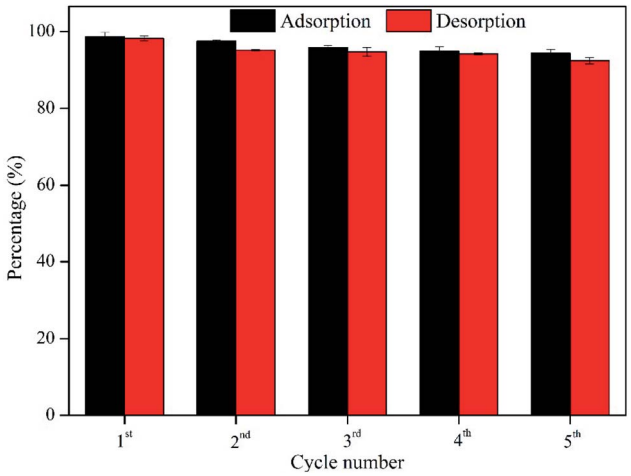

Fig. 10 Regeneration of PE/LG-CNTs-Ni/Al_2O_3 composite for Pb(II) adsorption.

of Pb(II) is conducted in the solution pH range of 2–6 (see Fig. 9) in the present study. It is hence inferred that electrostatic attraction between the negatively charged surface of PE/LG-CNTs-Ni/Al_2O_3 composite and positively charged Pb(II) would occur as the solution pH is relatively high (*i.e.*, 5.5 and 6). (3) π electron–cation interaction. It is reported that aromatic C=C of carbon materials is considered to be active sites for Pb(II) adsorption *via* π electron–cation interaction due to the delocalized π electron in C=C structure has good affinity with metal cations (Pb(II)).[43] FT-IR result in Fig. 4 shows that the C=C originated from the graphitic structure in CNTs can be seen in PE/LG-CNTs-Ni/Al_2O_3 composite, which hence may act as active sites for the adsorption of Pb(II). (4) Complexation with AlOH. Al_2O_3 can be considered as a high-efficient adsorbent to adsorption heavy metal ions according to the complexation between AlOH and metal ions.[45] In the present study, Al_2O_3 is employed as the substrate to prepare NiO/Al_2O_3 catalyst, which also is the major component of the PE/LG-CNTs-Ni/Al_2O_3 composite as evidenced by TPO analysis in Fig. 3a. As a result, the complexation between Pb(II) and AlOH originated from Al_2O_3 is responsible for the adsorption of Pb(II) to a certain degree.

$$\mathrm{Carbon}_{\mathrm{OH}}^{\mathrm{OH}} + \mathrm{Pb}^{2+} \rightarrow \mathrm{Carbon}_{\mathrm{O}}^{\mathrm{O}}\mathrm{Pb} + 2\mathrm{H}^{+} \quad (10)$$

$$\mathrm{Carbon}_{\mathrm{COOH}}^{\mathrm{COOH}} + \mathrm{Pb}^{2+} \rightarrow \mathrm{Carbon}_{\mathrm{COO}}^{\mathrm{COO}}\mathrm{Pb} + 2\mathrm{H}^{+} \quad (11)$$

$$\mathrm{Carbon}_{\mathrm{COOH}}^{\mathrm{OH}} + \mathrm{Pb}^{2+} \rightarrow \mathrm{Carbon}_{\mathrm{COO}}^{\mathrm{O}}\mathrm{Pb} + 2\mathrm{H}^{+} \quad (12)$$

3.3 Reusability

The reusability of an adsorbent greatly determines its cost and practical application prospect. According to the results presented above, PE/LG-CNTs-Ni/Al_2O_3 composite is found to be a superior adsorbent for the adsorption of Pb(II) in comparison with PE-CNTs-Ni/Al_2O_3 and LG-Chars-Ni/Al_2O_3 as well as other composites reported before. Accordingly, it is of significance to investigate the reusability of PE/LG-CNTs-Ni/Al_2O_3 composite. The result of five successive adsorption–regeneration cycles of PE/LG-CNTs-Ni/Al_2O_3 composite for Pb(II) adsorption is given in Fig. 10. As shown, the adsorption efficiency is 98.71%, 97.51%, 95.89%, 94.88% and 94.35% after the 1st, 2nd, 3rd, 4th and 5th cycle, respectively, indicating that PE/LG-CNTs-Ni/Al_2O_3 composite has excellent operating stability and is reusable.

4 Conclusions

Well-ordered CNTs, amorphous carbon and curved cone-shape CNTs are obtained from the catalytic reforming the pyrolysis volatiles of PE, LG and their mixture, respectively, using home-made NiO/Al_2O_3 as catalyst according to the results from SEM and TEM. The curved cone-shape CNTs from PE/LG mixture possessing a diameter range of 10–100 nm and a length range of 0.1–1 μm are abundant in structural defects and O-containing surface functional groups, such as C–O, C=O and –OH. Py-GC/MS result reveals that the volatiles of PE/LG mixture are mainly composed of hydrocarbons and oxygenated compounds, which are highly responsible for the production of the curved cone-shape CNTs with unique characteristics. The curved cone-shape CNTs-containing catalyst composite presents a superior adsorption capability towards Pb(II) when it is employed in Pb(II) removal. Adsorption isotherm and adsorption kinetic studies show that the adsorption process can be well simulated by the Langmuir isotherm and Pseudo-second-order model, demonstrating that the adsorption is subjected to a homogeneous and chemical process. The calculated maximum adsorption capacity is as high as 146.08 mg g^{-1}, which is much higher than most of the adsorbents reported. Moreover, thermodynamic analysis reveals that the adsorption is spontaneous and endothermic. The mechanism for the high-efficient adsorption of Pb(II) by CNTs-containing catalyst composite are attributed to the interactions including complexation with O-containing surface functional groups, electrostatic attraction, π electron–cation interaction and complexation with AlOH.

Author contributions

Zhanghong Wang and Kun Qin designed the idea and carried out experiment. Zhikang Wang, Dekui Shen and Chunfei Wu supervised the work. The manuscript was written through contributions of all authors.

Conflicts of interest

There are no conflicts to declare.

Acknowledgements

The authors greatly acknowledge the funding support from the projects supported by National Natural Science Foundation of China (Grant no. 51676047 and 41867048), Guizhou Provincial Science-technology Support Plan Projects in 2018 (Guizhou Science Support [2018]2807), the scientific research fund of

Guizhou Minzu University (GZMUZK[2021]YB13), the scientific research platform of Guizhou Minzu University (GZMUGCZX [2021]02) and the construction project of Key Laboratory of State Ethnic Affairs Commission ([2020] No. 91 of DDA office).

References

1 A. Talbi, Y. Kerchich, R. Kerbachi and M. Boughedaoui, *Environ. Pollut.*, 2018, **232**, 252–263.
2 Z. Wang, D. Shen, F. Shen, C. Wu and S. Gu, *J. Mol. Liq.*, 2017, **241**, 612–621.
3 N. Bortey-Sam, Y. Ikenaka, O. Akoto, S. M. M. Nakayama, K. A. Asante, E. Baidoo, C. Obirikorang, H. Mizukawa and M. Ishizuka, *Environ. Pollut.*, 2018, **235**, 163–170.
4 A. I. A. Sherlala, A. A. A. Raman, M. M. Bello and A. Asghar, *Chemosphere*, 2018, **193**, 1004–1017.
5 A. A. Ihsanullah, A. M. Al-Amer, T. Laoui, M. J. Al-Marri, M. S. Nasser, M. Khraisheh and M. A. Atieh, *Sep. Purif. Technol.*, 2016, **157**, 141–161.
6 X. Ren, C. Chen, M. Nagatsu and X. Wang, *Chem. Eng. J.*, 2011, **170**, 395–410.
7 Z. Wang, D. Shen, F. Shen, C. Wu and S. Gu, *J. Mol. Liq.*, 2017, **241**, 603–611.
8 S. K. Hubadillah, M. H. D. Othman, Z. Harun, A. F. Ismail, M. A. Rahman and J. Jaafar, *Ceram. Int.*, 2017, **43**, 4716–4720.
9 N. Kobylinska, D. Klymchuk, A. Shakhovsky, O. Khainakova, Y. Ratushnyak, V. Duplij and N. Matvieieva, *RSC Adv.*, 2021, **11**, 26974–26987.
10 Q. Liu, G.-L. Zang and Q. Zhao, *RSC Adv.*, 2021, **11**, 25880–25891.
11 Z. Wang, D. Shen, C. Wu and S. Gu, *Green Chem.*, 2018, **20**, 5031–5057.
12 L. Xu, S. Wang, J. Zhou, H. Deng and R. L. Frost, *Chem. Eng. J.*, 2018, **335**, 450–457.
13 W. N. Nyairo, Y. R. Eker, C. Kowenje, I. Akin, H. Bingol, A. Tor and D. M. Ongeri, *Sep. Sci. Technol.*, 2018, **53**, 1498–1510.
14 M. Yao, Z. Wang, Y. Liu, G. Yang and J. Chen, *Carbohydr. Polym.*, 2019, **212**, 345–351.
15 L. Cao, I. K. M. Yu, Y. Liu, X. Ruan, D. C. W. Tsang, A. J. Hunt, Y. S. Ok, H. Song and S. Zhang, *Bioresour. Technol.*, 2018, **269**, 465–475.
16 N. Yari Moghaddam, B. Lorestani, M. Cheraghi and S. Jamehbozorgi, *Water Environ. Res.*, 2019, **19**, 475–482.
17 C. Wu, J. Huang and P. T. Williams, *Int. J. Hydrogen Energy*, 2013, **38**, 8790–8797.
18 D. Xu, S. Yang, Y. Su, Y. Xiong and S. Zhang, *J. Hazard. Mater.*, 2021, **413**, 125289.
19 C. Wu, Z. Wang, P. T. Williams and J. Huang, *Sci. Rep.*, 2013, **3**, 2742.
20 C. Wu, Z. Wang, J. Huang and P. T. Williams, *Fuel*, 2013, **106**, 697–706.
21 D. Shen, J. Zhao, R. Xiao and S. Gu, *J. Anal. Appl. Pyrolysis*, 2015, **111**, 47–54.
22 C. Wu, Z. Wang, L. Wang, P. T. Williams and J. Huang, *RSC Adv.*, 2012, **2**, 4045–4047.
23 J. Alvarez, S. Kumagai, C. Wu, T. Yoshioka, J. Bilbao, M. Olazar and P. T. Williams, *Int. J. Hydrogen Energy*, 2014, **39**, 10883–10891.
24 C. Wu, Z. Wang, V. Dupont, J. Huang and P. T. Williams, *J. Anal. Appl. Pyrolysis*, 2013, **99**, 143–148.
25 A. Soomro, S. Chen, S. Ma, C. Xu, Z. Sun and W. Xiang, *Biomass Bioenergy*, 2018, **115**, 210–222.
26 Z. W. Pan, S. S. Xie, B. H. Chang, L. F. Sun, W. Y. Zhou and G. Wang, *Chem. Phys. Lett.*, 1999, **299**, 97–102.
27 H. Wang, Z. Xu, A. Kohandehghan, Z. Li, K. Cui, X. Tan, T. J. Stephenson, C. K. King'ondu, C. M. B. Holt, B. C. Olsen, J. K. Tak, D. Harfield, A. O. Anyia and D. Mitlin, *ACS Nano*, 2013, **7**, 5131–5141.
28 S. Tabesh, F. Davar and M. R. Loghman-Estarki, *J. Alloys Compd.*, 2018, **730**, 441–449.
29 S. Gillet, M. Aguedo, L. Petitjean, A. R. C. Morais, A. M. da Costa Lopes, R. M. Lukasik and P. T. Anastas, *Green Chem.*, 2017, **19**, 4200–4233.
30 C. Wu, M. A. Nahil, N. Miskolczi, J. Huang and P. T. Williams, *Environ. Sci. Technol.*, 2014, **48**, 819–826.
31 V. Fierro, V. Torné-Fernández and A. Celzard, *Microporous Mesoporous Mater.*, 2006, **92**, 243–250.
32 R. Bagri and P. T. Williams, *J. Anal. Appl. Pyrolysis*, 2002, **63**, 29–41.
33 W. Jin, D. Shen, Q. Liu and R. Xiao, *Polym. Degrad. Stab.*, 2016, **133**, 65–74.
34 K. A. Shah and B. A. Tali, *Mater. Sci. Semicond. Process.*, 2016, **41**, 67–82.
35 W.-J. Liu, H. Jiang and H.-Q. Yu, *Green Chem.*, 2015, **17**, 4888–4907.
36 L. Yu, Y. Lv, Y. Zhao and Z. Chen, *Mater. Lett.*, 2010, **64**, 2145–2147.
37 W. Zhang, S. Mao, H. Chen, L. Huang and R. Qiu, *Bioresour. Technol.*, 2013, **147**, 545–552.
38 L. Zhou, L. Ji, P.-C. Ma, Y. Shao, H. Zhang, W. Gao and Y. Li, *J. Hazard. Mater.*, 2014, **265**, 104–114.
39 I. A. A. Hamza, B. S. Martincigh, J. C. Ngila and V. O. Nyamori, *Phys. Chem. Earth*, 2013, **66**, 157–166.
40 D. K. Venkata Ramana, D. H. Kumar Reddy, B. N. Kumar, K. Seshaiah, G. P. Chandra Rao and C. Lu, *Sep. Sci. Technol.*, 2013, **48**, 403–412.
41 Z. Wang, D. Shen, F. Shen and T. Li, *Chemosphere*, 2016, **150**, 1–7.
42 Z. Wang, F. Shen, D. Shen, Y. Jiang and R. Xiao, *J. Environ. Sci.*, 2017, **53**, 293–300.
43 L. Fan, P. Chen, Y. Zhang, S. Liu, Y. Liu, Y. Wang, L. Dai and R. Ruan, *Bioresour. Technol.*, 2017, **225**, 199–205.
44 Z. Wang, G. Liu, H. Zheng, F. Li, H. H. Ngo, W. Guo, C. Liu, L. Chen and B. Xing, *Bioresour. Technol.*, 2015, **177**, 308–317.
45 W. Sun, K. Yin and X. Yu, *Chem. Eng. J.*, 2013, **225**, 464–473.